Tailored Hardness Profiles Through a Combination of Specialized PBF-LB Processing Strategies with Subsequent Heat Treatment for Graded High-Strength Components Made of Maraging Steel

Niki Nouri [1,*1], Gregor Graf [2], Sandipan Sen [1], Volker Schulze [1] and Stefan Dietrich [1]

[1] *Institute for Applied Materials – Materials Science and Engineering (IAM-WK) / Karlsruhe Institute of Technology (KIT), 76131 Karlsruhe, Germany*
[2] *Rosswag GmbH, 76327 Pfinztal, Germany*

This study investigates the utilization of laser powder bed fusion for fabricating functionally graded parts using a novel maraging steel named Specialis®. By manipulating the processing strategy involving single and synchronized dual laser exposures, along with remelting, graded parts are successfully produced. Both the as-built and heat-treated specimens exhibit hardness variations of up to 80 HV across distinct regions. Notably, a reversal of hardness levels occurs after heat treatment, with the originally harder as-built dual laser zone becoming the softest zone following the post heat treatment. This phenomenon is attributed to the early precipitation stage resulting in from the intrinsic heat treatment which occurs during the dual laser processing strategy, which leads to higher hardness in the dual laser as-built condition. However, upon aging, the peak hardness is attained uniformly across all regions. Thus, the higher proportion of austenite present in the dual laser zone, which was identified by means of x-ray diffraction and differential scanning calorimetry, lowers the hardness. Therefore, there is an intriguing shift regarding the area with the highest hardness. These findings offer innovative approaches and eliminate the necessity for complex and time-consuming intrinsic heat treatment steps. Instead, the manufactured parts can be efficiently furnace-hardened while retaining their graded properties. These findings facilitate the production of components with tailored hardness profiles, precisely suited for their intended applications. The versatility of additive manufacturing, combined with the unique capabilities of Specialis®, opens a new avenue for creating functionally graded parts with improved mechanical properties.

Keywords: *dual laser based powder bed fusion, maraging steel, post heat treatment, precipitation hardening, functionally graded material, tailored hardness*

1. Introduction

Functionally graded materials (FGMs) designate a group of advanced materials with a progressive variation in properties regarding the spatial positions by varying the material, microstructure, defects or macrostructure [1)]. The fabrication of metal FGMs by means of additive manufacturing (AM) has been of great interest in recent years, as the freedom in geometry during the process could simplify the approach and the flexible use of process parameters enables a specific adaption of components to the application (e.g. via different solidification conditions). Numerous studies have explored the gradation of parts fabricated by AM by varying the chemical composition [2)], the density [3)], the structure [4)], or the process parameters which result in a change in the microstructure [5)]. An intrinsic heat treatment (IHT) during the AM process could also change the microstructure and open new possibilities of creating FGMs, as already achieved for a maraging steel by controlled pausing between alternating layers [6)].

Maraging steels have been extensively investigated as suitable materials for laser powder bed fusion (PBF-LB) in the past decade. They are characterized by a ductile nickel-matensite matrix with a low amount of C with martensite finish temperature M_f usually between 200 and 300 °C. To achieve peak hardness, these high-strength steels must undergo a long aging heat treatment (~6 h) either directly from as-built state or after a solution heat treatment at ~850 °C. Precipitation hardening occurs during aging due to the formation of intermetallic phases such as Ni_3Mo, Ni_3Ti and Fe_2Mo [7–11)]. Nevertheless, there has been evidence of hardness increase after short aging times [12,13)] due to early precipitation formation [14)].

In this work a novel maraging steel for PBF-LB has been analyzed regarding the manufacturing of a graded microstructure by varying the processing strategies. Using an IHT combined with the short time aging effect enabled a targeted modification of the microstructure in as-built state. Differential scanning calorimetry (DSC), hardness measurements and X-ray crystallography were used to characterize each processing parameter zone in order to identify potential correlations between the processing parameters and the ensuing microstructure. Maraging steels manufactured by PBF-LB commonly find use in applications demanding complex geometries and high strength, such as molds. Therefore, the investigation of the graded parts were carried out before and after heat treatment. The primary inquiry was whether the grading, achieved through the variation of process parameters, could be maintained after heat treatment.

2. Experiment

2.1 Material

The investigated novel maraging steel, called Specialis®, has been developed for PBF-LB by SpecMaterials and processed by Rosswag Engineering. Table 1 contains the chemical composition of the material, which is based on the commonly used maraging steels 18Ni300 and 18Ni350, with an addition of V and Al. The focus of earlier investigations was on the optimization of material qualification process [15)], process parameters [16,17)], heat treatment [17)], as well as the analysis of phase transformations and strengthening mechanisms [18)]. Specialis® has a relative density of > 99.7 % and surpasses the hardness of conventional 18Ni300 by reaching ~700 HV after direct aging and ~760 HV after

*[1] PhD Student, Karlsruhe Institute of Technology (KIT)

solution treatment followed by aging, while requiring a shorter aging time of 2 h. The main strengthening effects observed after heat treatment include intermetallic precipitations and grain refinement.

Table 1: Chemical composition of Specialis® in wt%

C	Ni	Co	Mo	Ti	V	Al	Fe
0.01	18.27	10.69	4.22	1.75	1.61	0.19	Bal.

2.2. Processing Strategies

All samples were fabricated by the PBF-LB system SLM®280 HL Twin 400 W with gas flow upgrade by SLM Solutions Group AG. A schematic overview of the processing strategies and their influence on the thermal history of the melt pool is shown in Figure 1.

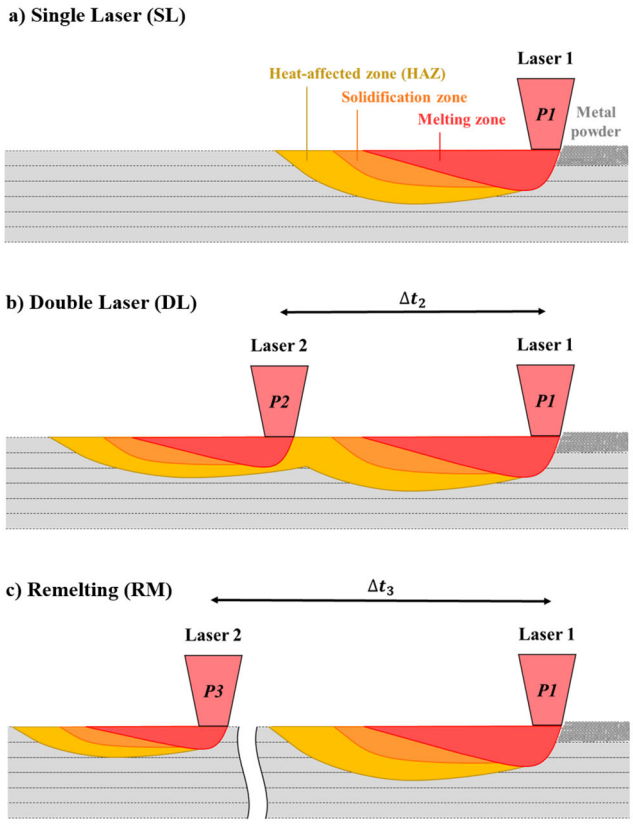

Figure 1: Overview of the setup and the influence of a) SL, b) DL, c) RM processing strategy on the thermal history of the melt pool and the layers underneath.

The following three processing strategies were used with the optimized parameters, derived from earlier studies [16,17]:

- Single laser (SL): only one laser with the power *P1* = 200 W is used.
- Dual laser (DL): A second laser with the power *P2* = 190 W follows the same path as the first laser with the power *P1*, keeping a constant time offset of Δt_2 = 6.25 ms to the first laser. This would extend the cooling time and the resulting IHT.
- Remelting (RM): The second laser has a reduced power of *P3* = 125 W compared to the DL strategy and the distance to the first laser is increased. There is a time offset of Δt_3 = 3 s between both lasers, allowing the material to reach a homogenous temperature level before the second laser approaches.

The following scanning parameters were kept constant for all strategies: 800 mm/s scanning speed, 85 µm hatch distance, and 40 µm layer thickness.

2.3 Methods

A DIL 805 dilatometer from TA Instruments was used to perform the short time aging heat treatments at 500 °C for 5, 10, 25, 50 and 100 s. The process involved inductive heating within a vacuum chamber filled with helium to prevent oxidation or evaporation. To regulate the temperature, a type S thermocouple was spot welded at the center of a 10 mm-long cylindrical hollow sample, fabricated with SL strategy.

To explore the feasibility of manufacturing graded components, cubic samples were vertically divided into three distinct zones, as visible in Figure 2. The fabrication was carried out by using three processing strategies in each layer. The chemical composition of these graded samples was determined using an iCAP 7600 DUO inductively coupled plasma-optical emission spectrometry (ICP-OES) instrument from Thermo Fisher Scientific. At least three samples per strategy were analyzed to obtain a mean value.

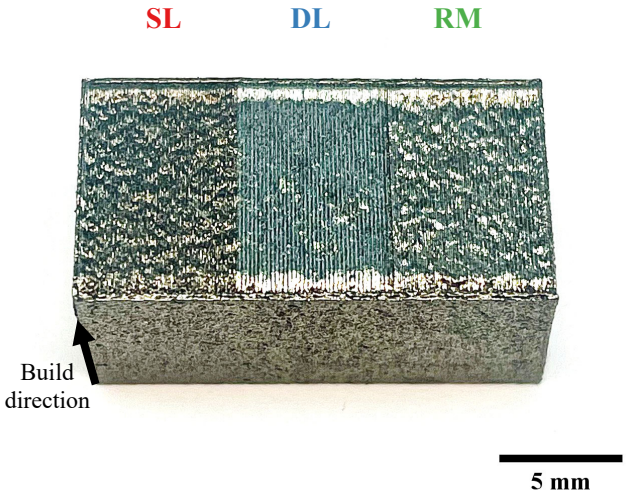

Figure 2: An example of a graded PBF-LB samples fabricated by using three different processing strategies (SL, DL, RM).

Micro Vickers hardness measurements at $HV_{0.1}$ were conducted on the same cubic samples using a Qness Q30a+ tester, following the DIN EN ISO 6507-1 standard [19]. The samples were ground and polished prior to the measurements. For each sample, three horizontal hardness profiles and one vertical profile per area (SL, DL, RM) were generated. The horizontal measurements started and ended 1 mm from the side edges to eliminate the influence of any boundary effects. For the same reason the vertical measurements started 0.5 mm below the top surface. The hardness has been measured both in as-built and heat treated states. Heat treated samples were subject to a vacuum furnace aging treatment at 500 °C for 3 h.

The γ-phase content was determined through X-ray diffraction (XRD) analysis using a Bruker D2 Phaser equipped with CuKa radiation. The scans encompassed a 2θ range spanning from 48 to 105 degrees, with a 0.01 step size.

Data analysis followed the ASTM E975 standard [20], employing a 6-line method to compute the integrated intensity of individual diffraction peaks (hkl). For the assessment of austenite, the {200}, {220}, and {311} diffraction peaks were used, while for martensite, the analysis was based on the {200}, {211}, and {220} diffraction peaks. Similar to the hardness measurement, both as-built and heat treated samples were examined.

Differential scanning calorimetry (DSC) was used to identify and characterize phase transformations by measuring heat flow differences as a Specialis® sample and an empty reference crucible were heated at a constant rate. A calibrated DSC 404 F1 Pegasus from Netzsch Gerätebau GmbH was employed in an Ar atmosphere (99.9999 % purity). For this investigation, a round sample with 6 mm diameter and 1 mm height was wire cut out of each region (SL, DL, RM). They were heated at 20 K/min up to 1000 °C, held for 15 minutes, and then naturally cooled in the furnace. Afterwards the same cycle has been repeated in order to compare the phase transformations of as-built state with a solution treated homogenized state.

3. Results

3.1 Phase Transformations

Figure 3 illustrates the results obtained through DSC analysis. In a previous study [18] it has been shown that the Specialis® DSC results contain two exothermic (1Exo and 2Exo) and two endothermic (3Endo and 4Endo) peaks. The first and second peak correspond to the cluster and precipitation formation, whereas the third and fourth peaks occur during the austenite reversion.

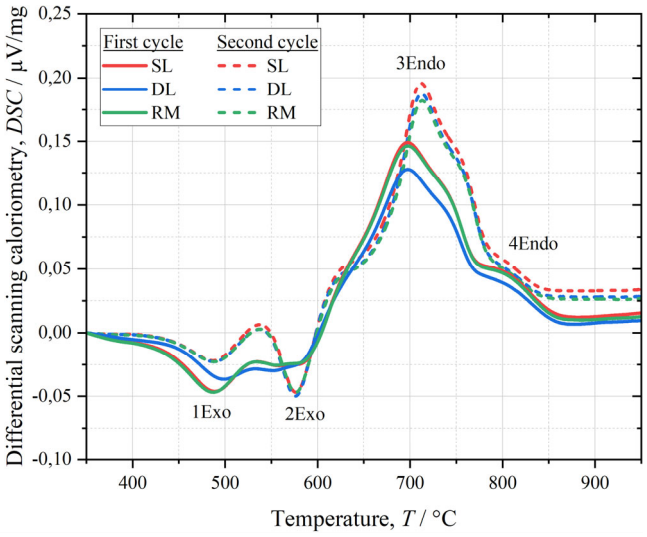

Figure 3: The results of the DSC investigations for all three processing strategies. The first cycle corresponds to the phase transformations of the as-built state upon heating, whereas the second cycle has a solution treated initial microstructure.

During the initial cycle, there is a notable resemblance in the thermal profiles of SL and RM, while DL demonstrates distinct characteristics. Specifically, DL exhibits reduced peak intensities across the entire temperature range in comparison to SL and RM, with the exception of 2Exo peak, which corresponds to the intermetallic precipitation formation. Moving into the second cycle, a convergence in the thermal profiles of DL with SL and RM is observed for all peaks, as the material has been homogenized through solution treatment of the first cycle. Overall, the second cycle shows an elevation in peak intensities when compared to the initial cycle.

3.2 Hardness Profiles

The outcomes of the horizontal hardness measurements conducted on graded components are exhibited in Figure 4. The position of the horizontal measurement (back, center, front) does not have any noteworthy influence on the hardness profile. Nevertheless, clear distinctions can be observed among the three employed processing approaches. While SL and RM exhibit comparable vertical mean hardness values in their as-built states (433±7 and 441±9 $HV_{0.1}$, respectively), DL results in a higher mean hardness (460±11 $HV_{0.1}$). These disparities become even more pronounced following heat treatment, wherein a surprising outcome arises: DL demonstrates a diminished mean hardness (629±18 $HV_{0.1}$) compared to SL and RM (712±11 and 703±18 $HV_{0.1}$, respectively). These trends remain consistent for samples produced with alternate sequences of processing strategy zones (DL|SL|RM or SL|RM|DL).

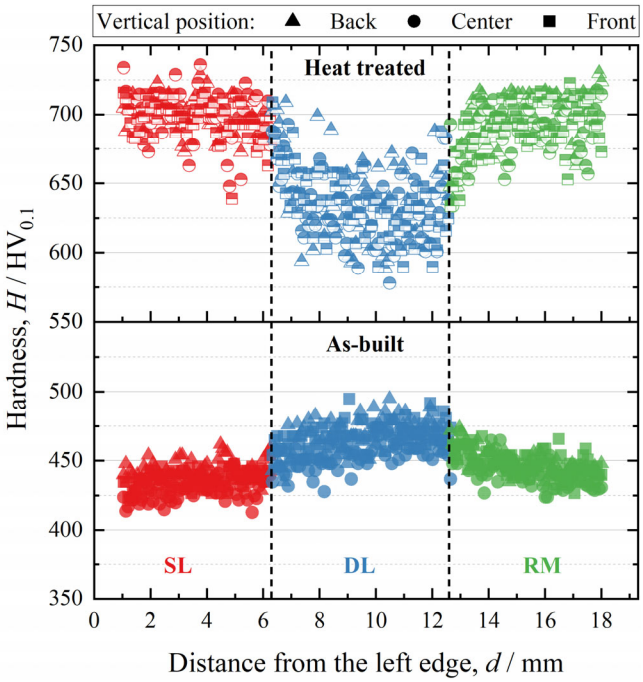

Figure 4: The horizontally measured hardness profiles of a sample in as-built and heat treated states at three different positions (back, center, front). Dashed lines approximately mark the transitions between different processing strategy zones (SL, DL, RM).

Short time aging treatments were carried out on SL samples in order to investigate potential early stages of precipitation hardening, which could occur during the fabrication process. The evolution of hardness over aging durations up to 100 s is depicted in Figure 5. The results clearly indicate that even brief aging times are enough to start the early stages of precipitation and induce an increase in hardness for Specialis® (~75 $HV_{0.1}$ after 10 s). The

relationship between the hardness H in $HV_{0.1}$ and the logarithm of aging time t_A in seconds can be described by the equation

$$H = 428 + 75\log(t_A),$$

illustrated as a grey dashed line in Figure 5. The intercept of this line with the y-axis at 428 aligns closely with the hardness value of the SL sample in its as-built state (433±7 $HV_{0.1}$).

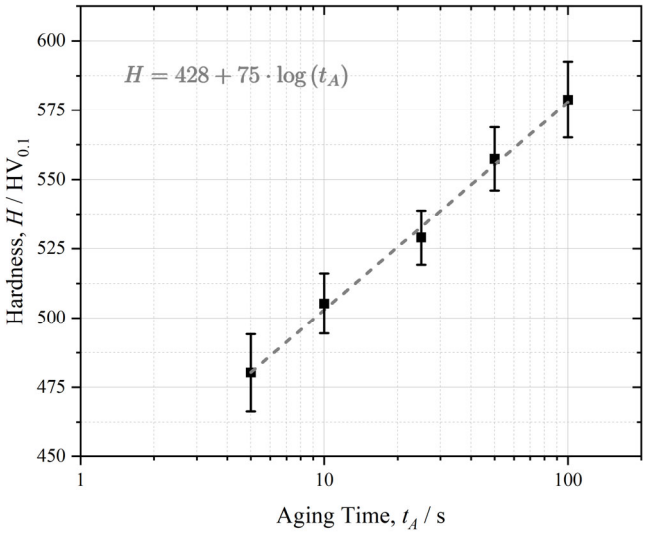

Figure 5: The evolution of hardness H depending on the aging time t_A after short time aging heat treatments of samples processed in the SL condition. The dashed grey line represents the linear fit between H and log (t_A) in seconds, which can be described by the equation written in the diagram.

3.3 Retained Austenite Amount

Figure 6 displays XRD diffractograms for both as-built and age hardened states of each processing parameter zone. The evaluated diffraction peaks are labeled at the bottom of the diagram. Upon initial observation it is notable that the heat treated samples have a significantly higher peak for the γ{200} reflection when compared to their as-built counterparts. Additionally, a higher γ{311} peak has been recorded for the DL sample compared to the other heat treated samples.

Using these diffractograms and the data analysis method mentioned in Section 2.3, the amount of retained austenite before and after heat treatment has been calculated for all three distinct zones. The results are listed in Table 2 for each processing parameter zone. In as-built state, both SL and RM samples contain a similar amount of γ-phase (~13 %), which is lower than in the DL sample (~21 %). The same tendency can be seen after the aging heat treatment at 500 °C for a duration of 3 h. However, in the heat-treated state, all samples show a substantial increase in austenite content (~40 % for SL and RM samples, and ~59 % for the DL sample). The increased standard deviation observed in the results after aging can be attributed to the utilization of samples with larger dimensions compared to the as-built state. This observation further elucidates the higher values measured in this work compared to those reported in the prior study [17].

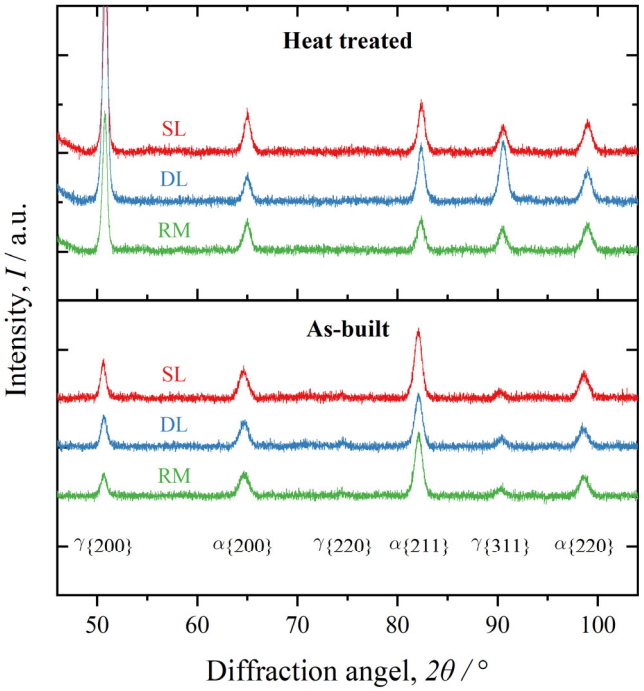

Figure 6: Recorded x-ray diffractograms for the determination of retained austenite amount in each processing zone, before and after aging heat treatment. The evaluated diffraction peaks for α-phase and γ-phase are noted in the diagram.

Table 2: Amount of γ-phase before and after heat treatment (HT) for all three processing parameter zones.

	γ-phase before HT [%]	γ-phase after HT [%]
SL	13.1 ± 5.6	40.2 ± 13.5
DL	21.0 ± 5.1	58.9 ± 13.4
RM	12.9 ± 4.4	40.0 ± 14.4

4. Discussion

In the context of the present study, the influence of three different manufacturing methods (SL, DL, RM) on the microstructural and mechanical characteristics of the material were examined, using graded components in as-built and heat treated states.

In its as-built state, DL offers a notably higher level of hardness (~460 $HV_{0.1}$) compared to SL and RM counterparts (~437 $HV_{0.1}$). This phenomenon can be attributed to the IHT generated by the second laser employed in the DL process, which leads to the early stages of precipitation hardening. This hypothesis is convincingly validated by the results obtained from short time aging experiments, wherein the hardness of SL specimens surpasses 500 $HV_{0.1}$, even following a mere 10 s aging at 500 °C. However, an unexpected deviation emerges after post-heat treatment, where DL's hardness (~629 $HV_{0.1}$) falls below that of SL and RM (~707 $HV_{0.1}$). In order to verify if any elements were evaporated due to high temperatures during PBF-LB fabrication process, a chemical analysis was carried out using ICP-OES. Yet the results showed no difference in the chemical composition of the three areas. Given the observed uniformity in the chemical composition, the diversion in hardness implies a modification within the microstructure of DL zone.

XRD investigations have provided an explanation about the mechanisms behind this intriguing shift. DL samples exhibit elevated contents of austenite phase both before and after aging heat treatment. In the as-built state, the melt pool does not undergo complete cooling during the DL strategy before the second laser initiates the first stages of aging. Consequently, less martensite is formed compared to SL and RM samples. This can also be seen in the DSC outcomes, where the DL sample results in a lower heat flow during the austenite reversion, which leads to the conclusion that less martensite is present for the phase transformation. It is worth mentioning that SL and RM samples also contain ~13 % retained austenite, primarily because the M_f of Specialis® is below room temperature and is thus inaccessible within this fabrication process [17]. However, the impact of the higher austenite content in the DL sample (~21 %) does not manifest in the hardness results due to the previously noted dominance of early stages of precipitation hardening. After undergoing an aging heat treatment, there is a notable increase in the amount of γ-phase due to Ni-segregation at grain boundaries, since Ni serves as an austenite stabilizer and promotes austenite reversion [21–23]. In this context, the elevated amount of austenite in the heat treated DL sample (~59 %) compared to SL and RM samples (~40 %) provides a plausible explanation for the observed reduction in hardness. In fact, the peak hardness of Specialis® is already attained after 2 h of aging [17], rendering the earlier precipitation hardening in the DL zone no longer significant and emphasizing the dominant influence of austenite content.

A few questions remain unanswered in the pursuit of understanding the distinctions between DL and other processing strategies. Firstly, a more in-depth exploration is needed to uncover the fundamental factors responsible for the reduced intensity of DSC peaks in DL samples during the initial cluster formation. Secondly, an analysis of the observed grain refinement effects in Specialis® [18] and their comparison to conventional maraging steels is essential in order to evaluate how different processing strategies impact the final microstructure of materials. To address these open questions and shed light on these disparities, comprehensive microstructural characterization is crucial. This approach should incorporate advanced techniques such as scanning electron microscopy coupled with energy dispersive x-ray spectroscopy and electron backscatter diffraction (SEM EDX and EBSD). Through these efforts, a better understanding of materials processing strategies and their implications can be achieved, ultimately leading to improved materials for various applications.

Nevertheless, leveraging the observed effects so far, a graded component was successfully manufactured, demonstrating the capability to preserve its graded microstructure even after undergoing heat treatment.

5. Conclusions

In Summary, this study involved the PBF-LB fabrication of graded components out of Specialis® maraging steel, utilizing three distinct manufacturing approaches: SL, DL, and RM. The following can be concluded:

- Despite having a higher amount of retained austenite in as-built state, DL showcased elevated initial hardness owing to early precipitation stages, a consequence of the IHT introduced by its second laser.
- In contrast, following heat treatment and the progression of precipitation hardening, both SL and RM exhibited superior hardness, although it was confirmed through chemical analysis that no significant amount of elements were evaporated during the processes.
- As peak hardness is already reached after 3 h of aging, the amount of austenite is the dominant effect after heat treatment, leading to the lower hardness of DL zone.
- Nevertheless, graded parts with a variation of up to ~80 $HV_{0.1}$ were successfully fabricated in as-built and heat treated states.

The findings open up the possibility of manufacturing complex geometries out of the maraging steel Specialis® with a graded microstructure, creating FGMs. For instance, it enables the achievement of surface hardening without incurring a hardness decline in overaged regions. Furthermore, the heat treatment can be performed throughout the entire part in a furnace, rather than being limited to the surface. This feature allows complex geometries to be topologically and metallurgically optimized to contain a tailored hardness profile specifically adapted to the application.

Acknowledgments

The authors would like to thank Dr. Thomas Bergfeldt from Institute for Applied Materials - Applied Materials Physics (IAM-AWP) / Karlsruhe Institute of Technology (KIT) for conducting the chemical analysis.

References

1) A. K. Mishra, K. Yadav, and A. Kumar: *Kumar, Mittal et al. (Hg.) 2022 – Advances in Additive Manufacturing:* pp. 281–297.

2) Y. Zhang, Z. Wei, L. Shi, and M. Xi, Journal of Materials Processing Technology **206** (2008) pp. 438–444.

3) M. Fousová, D. Vojtěch, J. Kubásek, E. Jablonská, and J. Fojt, Journal of the Mechanical Behavior of Biomedical Materials **69** (2017) pp. 368–376.

4) S. Y. Choy, C.-N. Sun, K. F. Leong, and J. Wei, Materials & Design **131** (2017) pp. 112–120.

5) T. Niendorf, S. Leuders, A. Riemer, F. Brenne, T. Tröster, H. A. Richard, and D. Schwarze, Adv. Eng. Mater. **16** (2014) pp. 857–861.

6) P. Kürnsteiner, M. B. Wilms, A. Weisheit, B. Gault, E. A. Jägle, and D. Raabe, Nature **582** (2020) pp. 515–519.

7) W. Spitzig, J. Chilton, and C. Barton: *Transactions of American Society for Metals*, ed. by J. Parina (ASM, Metals Park, Ohio, 1968) Vol. 60, pp. 635–639.

8) R. F. Decker and S. Floreen: *Maraging Steels: Recent Developments and Applications*: *Proceedings of the Symposium of TMS Annual Meeting*, ed. by R. Wilson (The Minerals, Metals & Materials Society, Warrendale, Pennsylvania, 1988) pp. 1–38.

9) W. Sha, A. Cerezo, and G. D. W. Smith, MTA **24** (1993)

pp. 1251–1256.
10) V. K. Vasudevan, S. J. Kim, and C. M. Wayman, MTA **21** (1990) pp. 2655–2668.
11) J. B. Lecomte, C. Servant, and G. Cizeron, J Mater Sci **20** (1985) pp. 3339–3352.
12) J. Marcisz and J. Stępień, Archives of Metallurgy and Materials **59** (2014) pp. 513–520.
13) A. Shekhter, H. I. Aaronson, M. R. Miller, S. P. Ringer, and E. V. Pereloma, Metall Mater Trans A **35** (2004) pp. 973–983.
14) E. V. Pereloma, R. A. Stohr, M. K. Miller, and S. P. Ringer, Metall Mater Trans A **40** (2009) pp. 3069–3075.
15) G. Graf, M. Neuenfeldt, T. Müller, J. Fischer-Bühner, D. Beckers, S. Donisi, F. Zanger, and V. Schulze, Advanced Materials Research **1161** (2021) pp. 27–36.
16) G. Graf, N. Nouri, S. Dietrich, F. Zanger, and V. Schulze, Materials (Basel, Switzerland) **14** (2021) pp. 4251.
17) N. Nouri, Q. Li, J. Damon, F. Mühl, G. Graf, S. Dietrich, and V. Schulze, Journal of Materials Research and Technology **18** (2022) pp. 931–942.
18) N. Nouri, Q. Li, R. Schneider, J. Damon, P. Schüßler, S. Laube, E. Müller, G. Graf, V. Schulze, and S. Dietrich, Materials Characterization **207** (2024) pp. 113522.
19) Deutsches Institut für Normung, *Metallische Werkstoffe - Härteprüfung nach Vickers. Teil 1: Prüfverfahren* [DIN EN ISO 6507-1] (2018).
20) ASTM International, *ASTM E 975, Practice for X-Ray Determination of Retained Austenite in Steel with Near Random Crystallographic Orientation* (West Conshohocken, PA, 2013).
21) H. Zhang, X. Ji, D. Ma, M. Tong, T. Wang, B. Xu, M. Sun, and D. Li, Journal of Materials Research and Technology **11** (2021) pp. 98–111.
22) U. K. Viswanathan, G. K. Dey, and V. Sethumadhavan, Materials Science and Engineering: A **398** (2005) pp. 367–372.
23) F. F. Conde, J. D. Escobar, J. P. Oliveira, M. Béreš, A. L. Jardini, W. W. Bose, and J. A. Avila, Materials Science and Engineering: A **758** (2019) pp. 192–201.